Article

Identifying the Metallic State of Rh Catalyst on Boron Nitride during Partial Oxidation of Methane by Using the Product Molecule as the Infrared Probe

Jikang Yao [†], Yuanjie Xu [†], Hua Yang, Zhuangzhuang Ren, Lizhi Wu * and Yu Tang *

Institute of Molecule Catalysis and In-Situ/Operando Studies, College of Chemistry, Fuzhou University, Fuzhou 350108, China
* Correspondence: wulz@fzu.edu.cn (L.W.); yu.tang@fzu.edu.cn (Y.T.)
† These authors contributed equally to this work.

Abstract: The partial oxidation of methane (POM) is a promising method for converting methane to syngas. The transition metal supported on boron nitride (BN) has recently been studied as part of a catalog of emerging catalysts. However, the chemical state of the metal supported on BN during methane reforming is still in debate. In this work, we report a rhodium catalyst on boron nitride (Rh/BN) for the POM, with exceptional activity and long-term stability at 600 °C for 230 h. The Rh/BN catalyst was investigated by X-ray diffraction, X-ray photoelectron spectroscopy, Raman spectroscopy, transmission electron microscopy, and diffuse reflectance infrared Fourier transformed spectroscopy (DRIFTS). As revealed by in situ DRIFTS, the infrared band (2020 cm^{-1}) of the product molecule, CO, adsorbed on the Rh, as the probe confirms the metallic state of Rh during the POM reaction. In addition, the results of in situ DRIFTS indicate that the reactive gaseous environment would react with the catalyst to form B-OH and B-H, which synergistically boost the POM activity.

1. Introduction

Syngas is one of the most important chemical intermediates, which may be utilized to generate hydrocarbons, alcohol, and other high-value chemicals via industrial processes such as the Fisher–Tropsch synthesis and methanol-to-olefin reactions [1–4]. As the primary component of natural gas, shale gas, and biogas, methane is a valuable resource that may be transformed to syngas by reforming reactions, such as steam reforming (SMR), dry reforming (DRM), and partial oxidation (POM) [5–9]. The partial oxidation of methane (POM) is featured for its mildly exothermic reaction ($\Delta H_{298K} = -37.8$ kJ mol^{-1}), resulting in reduced energy expenditure. Many efforts have been devoted to the development and investigation of the POM catalyst since the 1920s [10]. In generally, the conventional POM catalyst is based on a transition metal supported on an oxide, which is facing the disadvantages of deactivation during high temperature operation.

Boron nitride (BN) has emerged as a material for catalyst design in the last decade. BN is a binary compound composed of equal numbers of boron and nitrogen atoms. Hexagonal boron nitride (h-BN) has a typical layered structure similar to graphite. The h-BN has high mechanical strength, high thermal conductivity, and good lubricity. In addition, h-BN is chemically and thermally stable, making it a good choice for high-temperature catalytic processes [11–14]. The superior activity of h-BN as a catalyst in the oxidative dehydrogenation of ethane and propane has been reported, indicating that h-BN can potentially be employed as a catalyst or catalytic support in heterogeneous catalysis [15–18]. Dong et al. [19] reported that a catalyst of Ni metal was supported on an inert material boron nitride support, which was employed for methane dry reforming. Under the reaction atmosphere, amorphous BO$_x$ species are induced and migrated to Ni

metallic nanoparticles to form ultrathin BO_x overlayers. The B-O and B-OH sites on the surface of the BO_x overlayers work synergistically with the adjacent Ni sites to facilitate the reaction. In addition, Ni exists as metallic nanoparticles during the dry reforming of methane. However, Kim et al. [20] reported Rh was supported on BN catalysts for the POM reaction, which then elucidated the growth of single-phase Rh_2O_3 nanoparticles on BN. Given the reductive nature of the syngas product (CO and H_2), the chemical state of the supported metal on BN during methane reforming poses a concern.

In this work, Rh nanoparticles were loaded on a commercial nano h-BN support and applied to the partial oxidation of methane (POM) reaction to catalyze methane and oxygen to generate syngas ($CH_4 + 1/2O_2 = CO + 2H_2$). We have found that the Rh/BN catalyst exhibits superior activity and stability in the POM reaction. The conversion of methane and selectivity to CO are 63.4% and 79.2% at 600 °C and 89.9% and 88.8% at 750 °C, respectively. The catalytic activity remains well after tests on the time of stream for 230 h. The catalyst structure and reaction mechanism were studied by comprehensive characterizations. As revealed by the in situ DRIFTS spectrum, the metallic state of Rh during the POM reaction is confirmed by observing the infrared band of the product molecule, CO, which is adsorbed on the Rh as the probe. The results of in situ DRIFTS also suggest that the reactive gaseous environment would react with the catalyst to produce B-OH and B-H, which promote the POM activity synergistically. This work brings insights to the authentic state of the Rh/BN catalyst for methane reforming.

2. Results

As shown in Figure 1a, BN shows no activity for the partial oxidation of methane as the control experiment. Rh/BN exhibits activity for the POM reaction at 450 °C and high activity at high temperature. The conversion of methane over Rh/BN is 89.9% at 750 °C, which is much higher than that of BN (Figure 1b). Thus, Rh/BN is an outstanding catalyst for POM. Moreover, the catalyst was tested on the time of stream at 600 °C with a WHSV = 600,000 mL·g^{-1}·h^{-1}. Specifically, 45 mg of Rh/BN exhibits a conversion of 63.4% for methane (Figure 1c). The selectivity for producing H_2 and CO at 600 °C is 72.1% and 79.6%, respectively. After 230 h operation, there is only an ~8% decrease in the performance, in which the methane conversion decreases from 60.1% to 52.4%. This long-term stability suggests that the Rh/BN catalyst is promising for the POM reaction. In addition, the catalyst after the 230 h reaction was measured again, for the POM activity as the function of temperature (Figure 1d). The POM activity remains well after the long-term test.

X-ray diffraction pattern (XRD) and transmission electron microscopy (TEM) characterizations of Rh/BN are shown in Figure 2. The observed diffraction peaks at 26.8°, 41.6°, 43.9°, 55.2°, 71.4°, and 82.2° in the XRD patterns are indexed to the (002), (100), (101), (004), (104), and (112) planes of the hexagonal boron nitride (JCPDS-34-0421), respectively. No characteristic peaks of Rh_2O_3 or rhodium nanoparticle are detected, due to the low-loading of Rh. TEM images and element mapping show that Rh particles are evenly dispersed on BN after the POM reaction for 230 h, and the average size of the Rh particles is ~3.6 nm (Figure 2b–e). As compared in Figures 2e and S1, the average particle size of Rh NPs undergoes a slightly increase from 2.3 to 3.6 nm, after 230 h of the POM reaction at 600 °C. Therefore, it can be considered that the encapsulation overlayers act as a protective shell to stabilize the Rh NPs [21]. Meanwhile, no carbon deposition and metal sintering are observed in the TEM images of the catalyst used for partial oxidation of methane, which is consistent with the excellent stability of the catalyst. It is also worth noticing that, in Figure 2c, the Rh particles are encapsulated by ultrathin layers, which is attributed to the migration of boron oxide (BO_x) to the surface of the Rh particles. This phenomenon is consistent with reports on the strong metal support interaction (SMSI) between metal and BN [19,22,23].
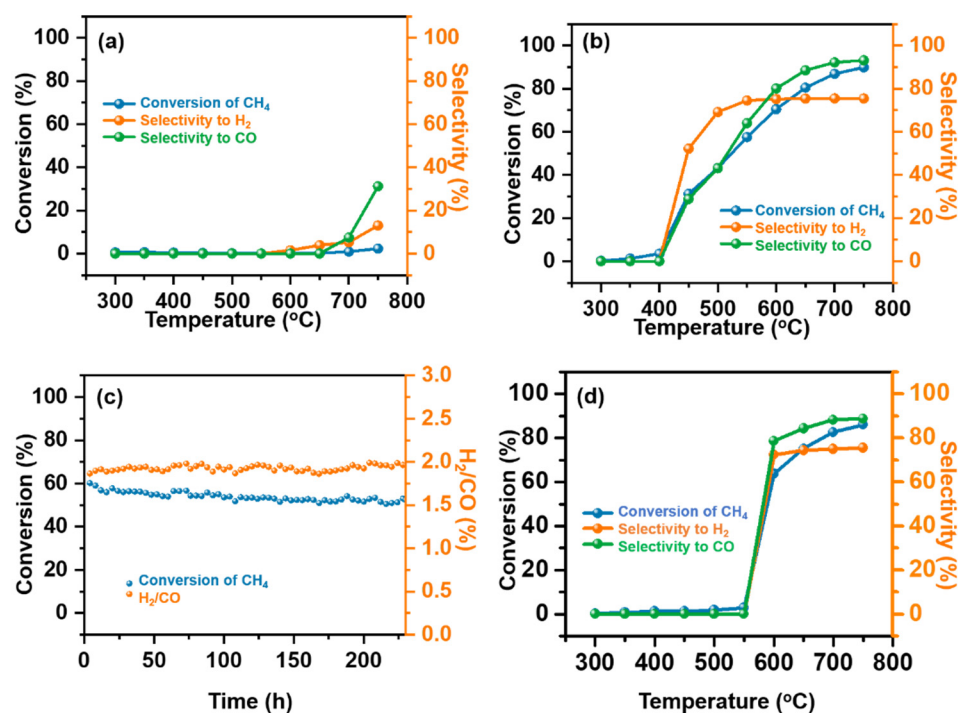
Figure 1. Temperature dependence of CH$_4$ conversion for POM over BN (**a**) and Rh/BN (**b**). Catalytic performance of Rh/BN for POM reaction at 600 °C against time on stream (**c**). The catalytic activity as the function of reaction temperature of the catalyst after 230 h long-term test (**d**). Test conditions: 50 mg of Rh/BN-fresh for (**a**,**b**,**d**), 45 mg for (**c**); the gas fed to the reactor is a mixture of 25 mL/min of 20% CH$_4$ and 25 mL/min of 10% O$_2$, and temperature is 600 °C.
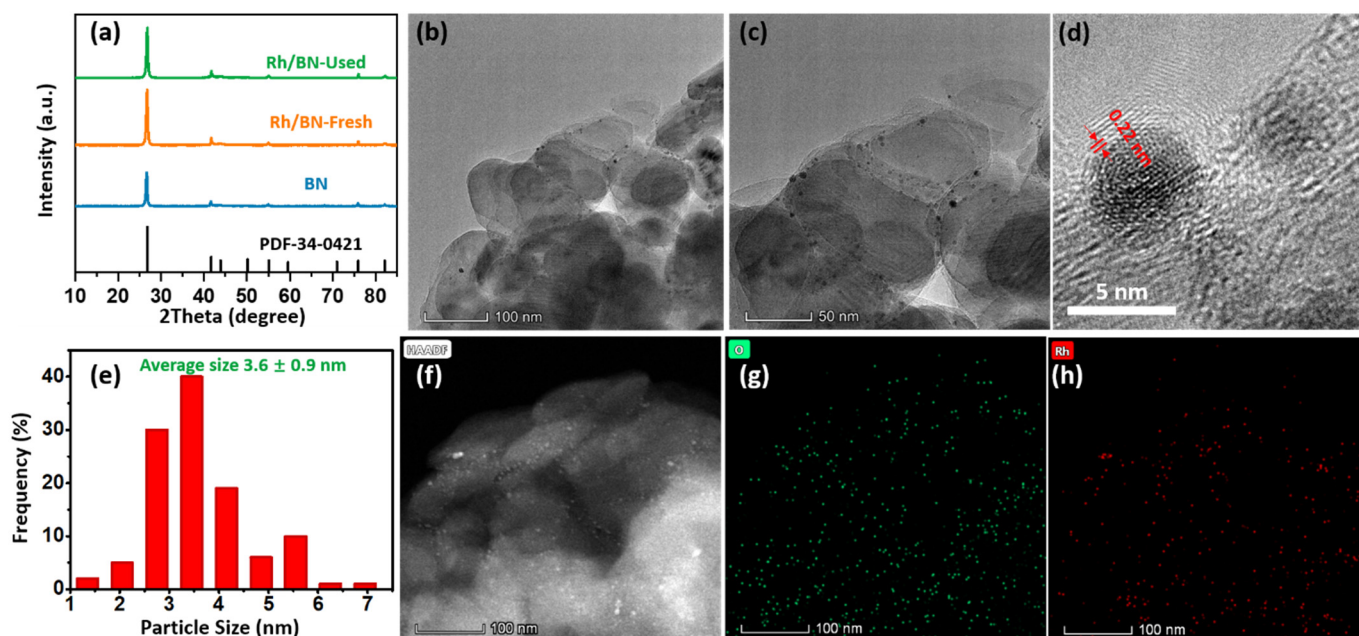
Figure 2. XRD patterns of BN, Rh/BN−Fresh, and Rh/BN−Used (**a**). TEM images of Rh/BN used for POM (**b**–**d**), the particle size distribution of Rh particles (**e**), and HAADF image (**f**) and element mapping of O (**g**) and Rh (**h**) obtained over the same area.

Raman spectroscopy and thermogravimetric characterization are the most effective methods to determine the carbon deposition of the catalyst. Generally, disordered carbon

and graphitic carbon appear at 1250–1350 and 1500–1700 cm^{-1}, respectively [24,25]. As shown in Figure 3a, only one peak at 1365 cm^{-1} is observed, which is assigned to the B-N band of the BN support [26]. No related carbon peaks appear in the used catalyst for partial oxidation of methane. Furthermore, no obvious weight loss is observed in the thermogravimetric curve of the catalyst used for the POM reaction, which also indicates that no coke is generated during the POM reaction (Figure 3b).
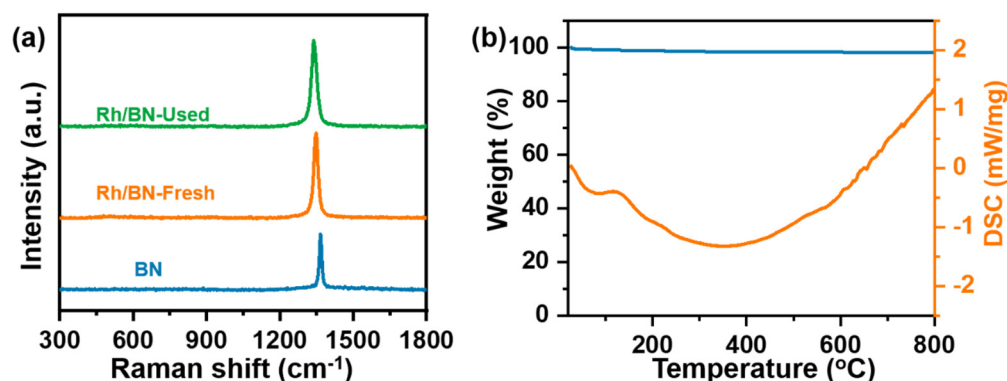
Figure 3. Raman spectra of BN, Rh/BN−Fresh, and Rh/BN−Used (**a**). TG−DSC of the spent Rh/BN catalyst (**b**).

The surface features of catalysts are studied by N$_2$ physical adsorption and X-ray photoelectron spectroscopy (XPS). The nitrogen adsorption–desorption isotherms of the catalysts are presented in Figure 4. The relevant analysis results are summarized in Table 1, including the specific surface areas by the Brunauer–Emmett–Teller (BET) method and porous texture information by the Barrett–Joyner–Halenda (BJH) method. The BET surface areas and average pore size of BN, Rh/BN-Fresh, and Rh/BN-Used are 30, 41, and 33 m^2/g and 19.7, 22.1, and 19.6 nm, respectively. The mesoporous structure is attributed to the stacking between BN nanoparticles. This shows that the specific surface area and pore size of the catalyst do not change after being used for partial oxidation of methane, indicating that the structure of the catalyst is stable.
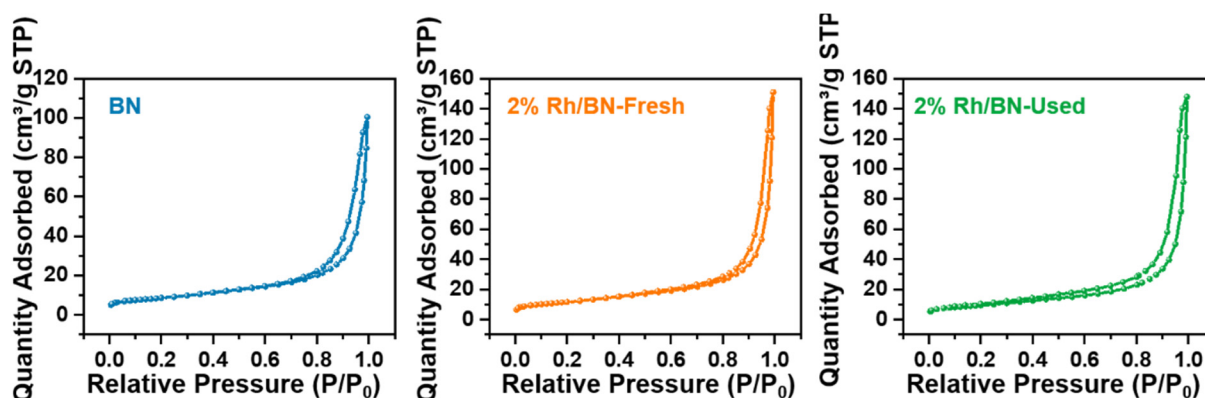
Figure 4. N$_2$ adsorption−desorption isotherms of BN, Rh/BN−Fresh, and Rh/BN−Used.

Table 1. BET specific surface areas of BN, Rh/BN−Fresh, and Rh/BN−Used.

Samples	BET Surface Area (m^2/g)	Pore Volume (cm^3/g)	Pore Size (nm)
BN	30	0.16	19.7
Rh/BN-Fresh	41	0.23	22.1
Rh/BN-Used	33	0.23	19.6

The XPS spectra of the Rh/BN-Fresh and Rh/BN-Used catalysts are shown in Figure 5. The O 1s spectra is deconvoluted to three main components at 530.8, 531.8, and 534.1 eV, which are assigned to the Rh-O bonding, B-O in the oxide, and the surface hydroxyl group of the catalyst, respectively [27,28]. Shoulder peaks at 192.0 eV in the B 1s spectra are assigned to B-O bonding, indicating the presence of boron oxide species [29]. The binding energy of Rh $3d_{5/2}$ of fresh Rh/BN at 309.3 eV (Rh^{3+}) suggests that there is a single fully oxidized Rh^{3+} state from the Rh_2O_3 species in the fresh catalyst. It can be observed that the Rh $3d_{5/2}$ in the Rh/BN catalyst used for the POM exhibits two valence states: an oxidation state corresponding to 309.3 eV (Rh^{3+}) and a metal state corresponding to 307.6 eV (Rh^0) [30]. The formation of Rh^0 is attributed to the reduction of rhodium oxide by a large amount of reductive gas (H_2 and CO) produced by the POM reaction. Furthermore, the XPS signal intensity of Rh in Rh/BN-Used is weaker than that of Rh/BN-Fresh, which could be attributed to the SMSI between Rh and BN in the form of BO_x patches on Rh during the POM process, which is consistent with the TEM results and the literature [19,22,31].
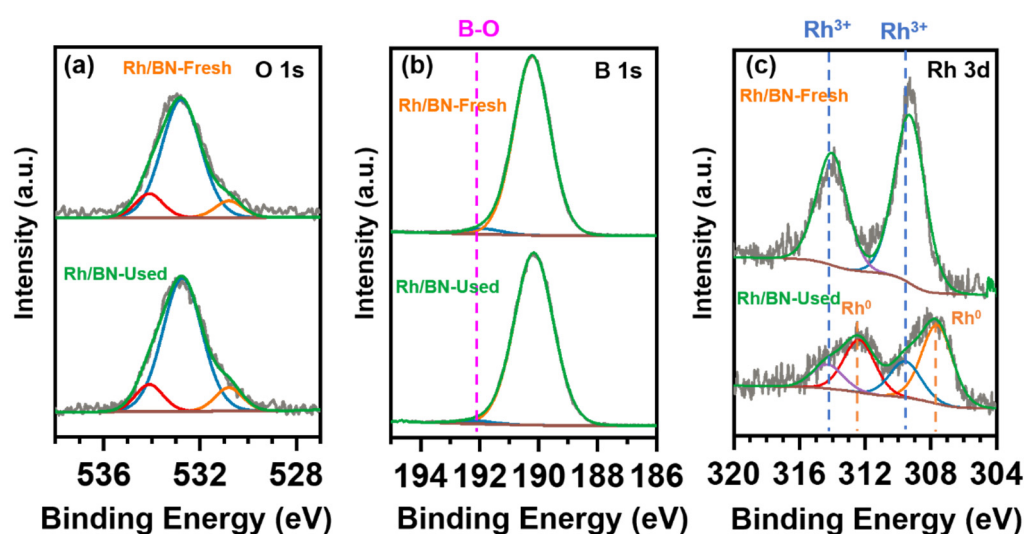

Figure 5. XPS spectra of Rh/BN-Fresh and Rh/BN-Used. O 1s (**a**), B 1s (**b**), and Rh 3d (**c**).

The encapsulation of Rh NPs by boron oxide during the catalytic process is further verified by diffuse reflectance infrared Fourier transform spectroscopy (DRIFTS). As shown in Figure 6, the status of Rh in the catalyst is examined by using external CO as the infrared probe [10,32–35]. The fresh Rh/BN catalyst shows the presence of four peaks at 2090, 2069, 2031, and 1908 cm^{-1}. The vibrational features at 2090 and 2030 cm^{-1} contribute to the gem-dicarbonyl [$Rh^+(CO)_2$] [36,37]. The peak at 2069 cm^{-1} is assigned to the C-O stretching vibration of the linear CO adsorption on the Rh atoms. The wide peak at 1908 cm^{-1} is assigned to the bridged adsorption on the neighboring Rh [38]. The infrared feature at 1908 cm^{-1} is a strong piece of evidence for the presence of metallic Rh nanoparticles. However, it is hard to find the CO adsorption on Rh in the Rh/BN used for the POM process. This suggests that Rh NPs cannot be exposed to the surface after the POM reaction. According to the above characterization results, the Rh NPs are encapsulated by boron oxide patches during the reaction process, to prevent CO adsorption on the Rh NPs [19,22,31]. To further confirm that the Rh NPs were wrapped, Rh/BN-Used catalyst was reduced at 300 °C in H_2 for 1 h, then cooled down to room temperature to carry out the DRIFT-CO experiment. As can be seen in Figure 6, the adsorption feature of CO on Rh/BN-Used appears at 2060 and 1919 cm^{-1} after reduction. This further proves that Rh particles are shielded with boron oxide during the POM process. The infrared band at 1919 cm^{-1} suggests the existence of metallic Rh, while the intensive and broad band at 2060 cm^{-1} indicates that the adsorption geometry of gem-dicarbonyl is not favored. It is

interpreted that the access of CO molecules to the surface Rh atoms is steric-restricted by BO_x patches [19,22,31].
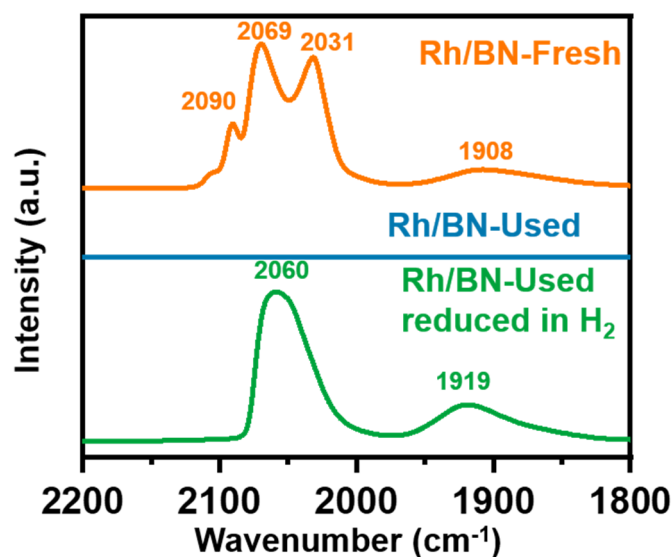
Figure 6. DRIFT$-$CO of Rh/BN$-$Fresh, Rh/BN$-$Used, and Rh/BN$-$Used reduced at 300 °C in H_2 for 1 h.

The chemical state and functional group on the surface of the catalyst are also investigated by in situ DRIFTS [32]. Three sets of in situ DRIFTS experiments are performed, as shown in Figure 7. No external CO is introduced in the experiment. The first experiment is monitoring the infrared spectrum on the time of stream under the POM reactive conditions (Figure 7a,b). Upon exposure to the POM atmosphere at 500 °C, the characteristic band of the hydroxyl stretching vibration is clearly observed at 3380 cm^{-1} (Figure 7a) [39,40]. Meanwhile, the emergence of B-H stretching (2480 cm^{-1}) is observed in Figure 7b [41]. Both results suggest that the hydrogen on methane is abstracted by the B atom, and the active methyl radical should be stabilized by the adjacent nitrogen atoms [42,43]. Moreover, the peak at 2021 cm^{-1} is observed for the C-O stretching vibration of molecule CO adsorption on Rh, in the manner of linear geometry. The wavenumber of 2021 cm^{-1} represents a typical linear adsorbed CO on the Rh atoms. Moreover, a minor infrared band at 1890 cm^{-1} is also observed for the CO that is adsorbed on two adjacent Rh atoms with the bridge geometry. Both infrared bands (2021 and 1890 cm^{-1}) demonstrate that the Rh catalyst adsorbs the molecule CO as the infrared probe, which is formed during the POM reaction [32]. These observations suggest that the catalyst was reduced to a metallic state during the POM reaction. Moreover, the BO_x encapsulation overlayers can be supposed to suppress sintering of Rh NPs. As shown in Figures 1 and S1, the average particle size of Rh NPs undergoes a slight increase from 2.3 to 3.6 nm after 230 h, over the POM reaction at 600 °C. Therefore, it can be considered that the BO_x encapsulation overlayers act as a protective shell to stabilize Rh NPs [20].

The key role of B-OH and B-H in POM process is further explored in the following two sets of DRIFTS experiments, as shown in Figure 7c–h. The catalyst is first exposed to argon atmosphere (Figure 7c,d), while no B-OH or B-H is observed. Then, 22.4 mL of CH_4 and O_2 are pulsed into the cell, while the infrared bands of B-OH and B-H appear immediately. More interestingly is that the B-OH (3480 cm^{-1}) does not disappear at 500 °C in flowing Ar. Therefore, the B-OH and B-O structure are confirmed during the POM reaction. Moreover, the infrared band at c.a. 2020 cm^{-1} is observed in the second set of in situ DRIFTS experiment, again suggesting the formation of metallic Rh nanoparticles. To further investigate whether B-OH would remain on the catalyst surface, the third DRIFT experiment is carried out (Figure 7e–f). The catalyst is exposed to O_2, then 22.4 mL CH_4 is dosed to the cell. It is noted that B-OH appears and gradually decreases with time. The

weak signal of B-H should be due to the large amount of oxygen in this experiment, which promotes the transformation of B-H. This evidence demonstrates that B-OH and B-H could participate in the POM catalysis. In addition, the infrared band of 2020 cm^{-1} is confirmed. As reported in the literature [44], methane dissociation occurred on reduced metal sites, and OH occurred on the support act as an oxygen source onto the Rh NPs. Therefore, according to the above analysis, it can be suggesting that B-OH and B-H sites on the BO_x encapsulation overlayers, together with surface Rh NPs sites, synergistically catalyze the surface POM process.
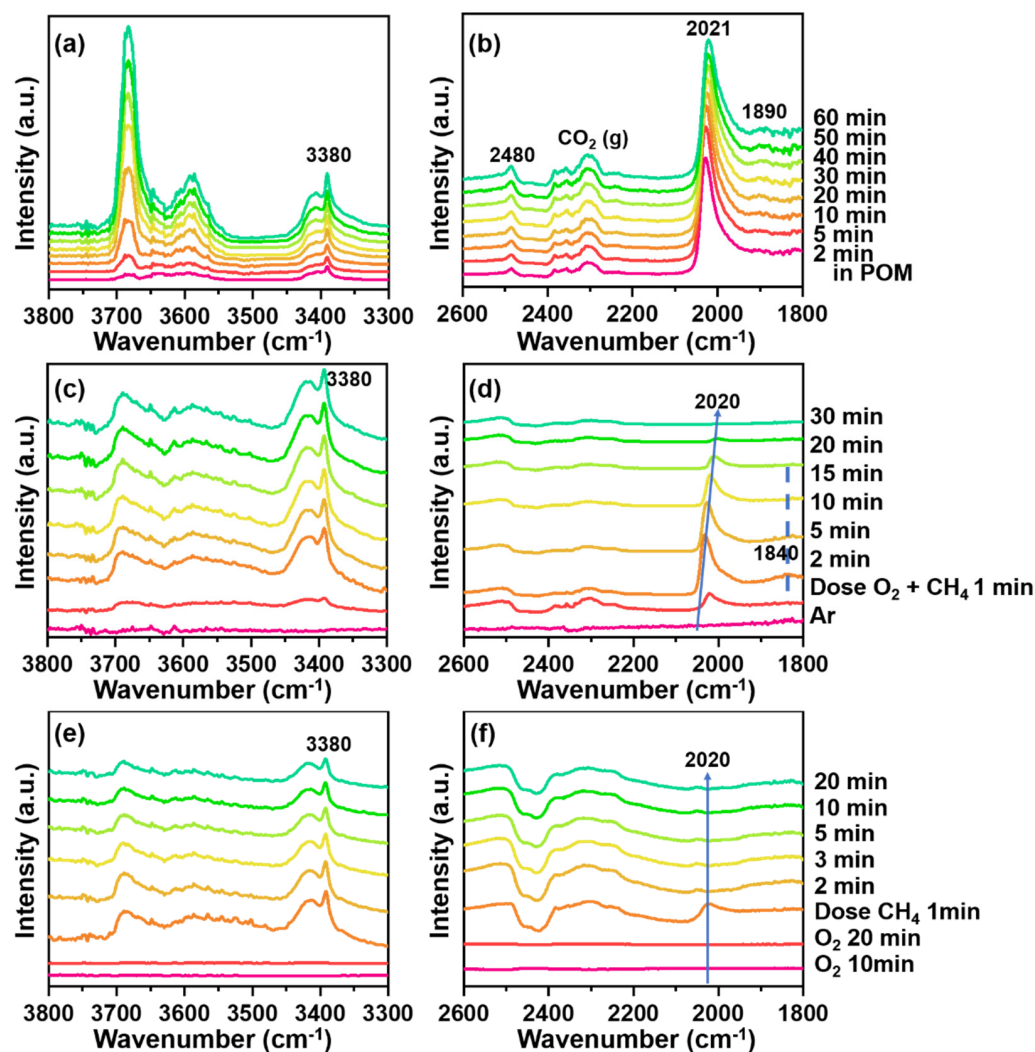
Figure 7. In situ DRIFT studies of Rh/BN at 500 °C with flowing CH_4 and O_2 stream in the range of 3800 to 3300 cm^{-1} (**a**) and in the range of 2600 to 1800 cm^{-1} (**b**). In situ DRIFT over Rh/BN at 500 °C with flowing Ar for stabilize, then pulse 22.4 mL CH_4 and O_2 and collect the spectra. Range of 3800 to 3300 cm^{-1} (**c**) and range of 2600 to 1800 cm^{-1} (**d**). In situ DRIFT over Rh/BN at 500 °C with flowing O_2 to stabilize, then pulse 22.4 mL CH_4 and collect the spectra. Range of 3800 to 3300 cm^{-1} (**e**) and range of 2600 to 1800 cm^{-1} (**f**).

3. Discussion

Based on the characterization and in situ DRIFTS results, Rh nanoparticles are proposed to be the active sites for the reaction. Therefore, we conclude that the reaction mechanism in this work is similar to those reported in the previous literature for the POM over a supported Rh nanoparticle catalyst [44,45]. Methane dissociation occurred on the

reduced metal sites, and OH occurred on the support act as an oxygen source onto the Rh NPs.

Besides the observation of B-O and B-H during the POM reaction, the key discovery of this work is the observation of an adsorbed CO band at ~2020 cm^{-1} during all three sets of in situ DRIFTS experiments. In the in situ DRIFT study of Figure 7, there is no external CO introduced into the reaction cell. In other words, all the CO observed is formed by the POM reaction proximal to the surface of the catalyst. Therefore, the product molecule, CO, serves as the infrared probe to investigate the chemical state of the Rh catalysts [32]. The wavenumbers, of 2020–2021 and 1840–1890 cm^{-1}, of the adsorbed CO are very close to the 2010 cm^{-1}, as reported in our recent work [32], which is also the probe of the infrared band of the product molecule CO on the Rh clusters on ceria. This observation suggests the Rh catalyst is metallic nanoparticles. However, it has been reported very recently that a supported single phase corundum-Rh_2O_3 is formed during the POM reaction and contributes to the POM activity [30], which poses the question of whether the metallic or oxide phase of the transition metal is the authentic catalyst for methane reforming, when Rh is supported on BN. Therefore, the observation of metallic Rh by using product molecule CO in this work brings new insight to this topic.

4. Materials and Methods

Catalyst preparation. Rh/BN catalyst was prepared by a wetness-impregnation method [46]. In a typical preparation of a 2 wt% Rh/BN catalyst, 0.2 g rhodium nitrate solution (containing 10% $Rh(NO_3)_3$, Aladdin, Shanghai, China) was added to 1.5 mL deionized water. Next, 1 g boron nitride (Boron nitride, Sigma-Aldrich, St. Louis, MO, USA, 99% trace metals basis, <150 nm avg. part. size) was added into a beaker. Then, the rhodium nitrate solution was dropped with stirring, until all the solution was mixed with the boron nitride. The slurry was dried in an oven at 60 °C overnight. The obtained sample was calcined at 500 °C for 5 h. To distinguish the different catalysts, fresh Rh/BN catalyst is named as Rh/BN-Fresh (or Rh/BN-f), while Rh/BN catalyst used for partial oxidation of methane is named as Rh/BN-Used (or Rh/BN-u).

Catalyst characterization. X-ray diffraction (XRD) was collected on a Smart Lab SE diffractometer (Rigaku, Tokyo, Japan) equipped with Cu Kα (λ = 1.5406 Å) X-ray source operating at 40 kV and 25 mA. The diffraction signal was collected with a HyPix-400(H) detector in the range of 10° < 2θ < 90°, with a scan speed of 5° per minute. Raman spectroscopy measurements were recorded on a DXRxi Raman microscope (Thermo Fisher Scientific, Waltham, MA, USA), with a laser of 532 nm wavelength. The Raman shift values were measured over the range from 400 to 3100 cm^{-1}. Transmission electron microscope (TEM) images and the energy-dispersive spectrum (EDS) were collected on FEI Talos F200S microscope (FEI, Hillsboro, OR, USA) at 200 kV. Temperature programed reduction and desorption were carried on an AutoChem II 2920 chemisorption apparatus (Micrometrics, Norcross, GA, USA), with a thermal conductivity detector (TCD). X-ray photoelectron spectrum (XPS) was collected on a Thermo Scientific ESCALAB 250 (Thermo Fisher Scientific, Waltham, MA, USA), and the data were acquired by a monochromatized Al Kα X-ray source (200 W). The binding energies were referenced to the C 1s peak of environmental carbon at 284.6 eV. The surface area and pore structure parameters of catalysts were analyzed by N_2 adsorption–desorption isotherms at 77 K on a Micromeritics ASAP 2020 (Micromeritics, Norcross, GA, USA). Before measurement, the samples were preheated under vacuum at 300 °C for 4 h.

The diffuse reflectance infrared Fourier transform spectroscopy (DRIFTS) measurements were performed by an iS50 FT-IR spectrometer (Thermo-Fisher, Waltham, MA, USA), with a mercury cadmium telluride (MCT) detector and a Harrick diffuse reflectance accessory (Harrick Scientific Product, New York, NY, USA). The reaction chamber was equipped with a ZnSe dome. Each spectrum was recorded with 32 scans at a resolution of 4 cm^{-1}. The catalyst was mounted in the cell without dilution.

In the typical protocol of DRIFTS, by using external CO as the probe (Figure 6), the fresh Rh/BN catalyst was pretreated at 300 °C for 30 min by 10% H_2/Ar, then cooled down to room temperature in flowing Ar. A spectrum was obtained as background. Then, CO (10%) was introduced, and the excess CO was purged with Ar. For the used Rh/BN, it was pretreated in Ar at 300 °C for 30 min before performing CO chemisorption experiment.

The protocol of in situ DRIFTS over Rh/BN is under partial oxidation of methane. The catalyst was pretreated at 300 °C for 1 h by 10% H_2/Ar. Then, after being heated up to 500 °C in flowing argon, a spectrum was collected as background. O_2 and CH_4 were introduced, and the spectra was collected every minute (Figure 7a,b). Furthermore, there was a series of DRIFTS experiments of dosed CH_4 and/or O_2 into the cell (Figure 7c–f).

Catalytic performance test. The catalytic performance of partial oxidation of methane was evaluated in a fixed bed quartz tubular reactor. The pelleting catalysts (40–60 mesh) were loaded in a quartz tube with an inner diameter of 6 mm. The reaction gas composition was 5% O_2, 10% CH_4, and 85% Ar. The flow rate of the total reactant was 50 mL/min. A K-type thermal couple coated with quartz shield was inserted into the catalyst bed to monitor the reaction temperature. The products were analyzed by an on-line chromatography (GC-2014, Shimazu, Kyoto, Japan), equipped with an auto-sampler; a line is HP-AL/S column (0.53 mm × 15 μm × 50 m) with flame ionization detector (FID), another is P-N (3.2 mm × 2.1 mm × 1.0 m) and MS-13X (3.2 mm × 2.1 mm × 3.0 m) column with thermal conductivity detector (TCD). $[CH_4]_{in}$ is the concentration of POM reaction without catalyst at room temperature, and the concentration of $[CH_4]_{out}$, $[CO]$, and $[H_2]$ during the POM reaction at different temperature is obtained by GC. The conversion of CH_4, and selectivity to H_2 and CO, are calculated as the following equations.

$$\text{Conversion (CH}_4) = \frac{[CH_4]_{in} - [CH_4]_{out}}{[CH_4]_{in}} \tag{1}$$

$$\text{Selectivity (H}_2) = \frac{\frac{1}{2} * [H_2]}{([CH_4]_{in} - [CH_4]_{out})} \tag{2}$$

$$\text{Selectivity (CO)} = \frac{[CO]}{[CH_4]_{in} - [CH_4]_{out}} \tag{3}$$

Catalytic performance of BN and Rh/BN were evaluated at temperatures varying from 300 to 750 °C under a flow of a mixture of 25 mL/min 20% CH_4 and 25 mL/min 10% O_2. For the measurements of catalytic performance, 50 mg of catalyst diluted with 300 mg of purified quartz was loaded into the reactor. The catalyst was heated up to 300 °C under the reaction mixture. During the test, each temperature was maintained for 2 h, and the outlet of reactor was detected by an on-line gas chromatography (the outlets of reactor were automatically collected every 20 min by on-line chromatography). Each temperature was tested six times and the data were stable. The average value of the six measured times was taken as the reported data.

5. Conclusions

In summary, Rh/BN is found to be an effective catalyst for the partial oxidation of methane (POM) with a long durability. During the POM process, Rh NPs are reduced by the product atmosphere and encapsulated by ultrathin boron oxide overlayers derived from the BN support. Our observations with in situ diffuse reflectance infrared Fourier transform spectroscopy (DRIFTS) offer important messages towards the understanding of the POM reaction. In situ DRIFTS characterization reveals that B-OH and B-H site are generated in the POM catalysis, which work synergistically with Rh sites to promote the POM process. These findings shed a light on the authentic state of the supported metal on BN during methane reforming.

Author Contributions: J.Y.: investigation, formal analysis; writing—original draft; Y.X.: investigation, formal analysis; writing—original draft, writing—review and editing; H.Y.: investigation, formal analysis; Z.R.: formal analysis; L.W.: formal analysis, writing—review and editing; Y.T.: conceptualization, writing—review and editing, supervision. All authors have read and agreed to the published version of the manuscript.

Institutional Review Board Statement: Not applicable.

Informed Consent Statement: Not applicable.

Data Availability Statement: Not applicable.

Conflicts of Interest: The authors declare no conflict of interest.

References

1. Pan, X.; Jiao, F.; Miao, D.; Bao, X. Oxide–Zeolite-Based Composite Catalyst Concept That Enables Syngas Chemistry beyond Fischer–Tropsch Synthesis. *Chem. Rev.* **2021**, *121*, 6588–6609. [CrossRef]
2. Wei, J.; Yao, R.; Han, Y.; Ge, Q.; Sun, J. Towards the development of the emerging process of CO_2 heterogenous hydrogenation into high-value unsaturated heavy hydrocarbons. *Chem. Soc. Rev.* **2021**, *50*, 10764–10805. [CrossRef] [PubMed]
3. Luk, H.T.; Mondelli, C.; Ferré, D.C.; Stewart, J.A.; Pérez-Ramírez, J. Status and prospects in higher alcohols synthesis from syngas. *Chem. Soc. Rev.* **2017**, *46*, 1358–1426. [CrossRef]
4. Bao, J.; Yang, G.; Yoneyama, Y.; Tsubaki, N. Significant Advances in C1 Catalysis: Highly Efficient Catalysts and Catalytic Reactions. *ACS Catal.* **2019**, *9*, 3026–3053. [CrossRef]
5. Aramouni, N.A.K.; Touma, J.G.; Tarboush, B.A.; Zeaiter, J.; Ahmad, M.N. Catalyst design for dry reforming of methane: Analysis review. *Renew. Sustain. Energy Rev.* **2018**, *82*, 2570–2585. [CrossRef]
6. Jang, W.-J.; Shim, J.-O.; Kim, H.-M.; Yoo, S.-Y.; Roh, H.-S. A review on dry reforming of methane in aspect of catalytic properties. *Catal. Today* **2019**, *324*, 15–26. [CrossRef]
7. Li, M.; Sun, Z.; Hu, Y.H. Catalysts for CO_2 reforming of CH_4: A review. *J. Mater. Chem. A* **2021**, *9*, 12495–12520. [CrossRef]
8. Tang, Y.; Li, Y.; Tao, F. Activation and catalytic transformation of methane under mild conditions. *Chem. Soc. Rev.* **2022**, *51*, 376–423. [CrossRef]
9. Tang, Y.; Wei, Y.; Wang, Z.; Zhang, S.; Li, Y.; Nguyen, L.; Li, Y.; Zhou, Y.; Shen, W.; Tao, F.F.; et al. Synergy of Single-Atom Ni1 and Ru1 Sites on CeO_2 for Dry Reforming of CH_4. *J. Am. Chem. Soc.* **2019**, *141*, 7283–7293. [CrossRef]
10. Tang, Y.; Fung, V.; Zhang, X.; Li, Y.; Nguyen, L.; Sakata, T.; Higashi, K.; Jiang, D.-E.; Tao, F.F. Single-Atom High-Temperature Catalysis on a Rh1O5 Cluster for Production of Syngas from Methane. *J. Am. Chem. Soc.* **2021**, *143*, 16566–16579. [CrossRef]
11. Belgamwar, R.; Rankin, A.G.M.; Maity, A.; Mishra, A.K.; Gómez, J.S.; Trébosc, J.; Vinod, C.P.; Lafon, O.; Polshettiwar, V. Boron Nitride and Oxide Supported on Dendritic Fibrous Nanosilica for Catalytic Oxidative Dehydrogenation of Propane. *ACS Sustain. Chem. Eng.* **2020**, *8*, 16124–16135. [CrossRef]
12. Liu, Z.; Yan, B.; Meng, S.; Liu, R.; Lu, W.-D.; Sheng, J.; Yi, Y.; Lu, A.-H. Plasma Tuning Local Environment of Hexagonal Boron Nitride for Oxidative Dehydrogenation of Propane. *Angew. Chem. Int. Ed.* **2021**, *60*, 19691–19695. [CrossRef]
13. Cao, Y.; Maitarad, P.; Gao, M.; Taketsugu, T.; Li, H.; Yan, T.; Shi, L.; Zhang, D. Defect-induced efficient dry reforming of methane over two-dimensional Ni/h-boron nitride nanosheet catalysts. *Appl. Catal. B Environ.* **2018**, *238*, 51–60. [CrossRef]
14. Bu, K.; Kuboon, S.; Deng, J.; Li, H.; Yan, T.; Chen, G.; Shi, L.; Zhang, D. Methane dry reforming over boron nitride interface-confined and LDHs-derived Ni catalysts. *Appl. Catal. B Environ.* **2019**, *252*, 86–97. [CrossRef]
15. Shi, L.; Wang, Y.; Yan, B.; Song, W.; Shao, D.; Lu, A.-H. Progress in selective oxidative dehydrogenation of light alkanes to olefins promoted by boron nitride catalysts. *Chem. Commun.* **2018**, *54*, 10936–10946. [CrossRef]
16. Shi, L.; Wang, D.; Song, W.; Shao, D.; Zhang, W.-P.; Lu, A.-H. Edge-hydroxylated Boron Nitride for Oxidative Dehydrogenation of Propane to Propylene. *ChemCatChem* **2017**, *9*, 1788–1793. [CrossRef]
17. Grant, J.T.; Carrero, C.A.; Goeltl, F.; Venegas, J.; Mueller, P.; Burt, S.P.; Specht, S.E.; McDermott, W.P.; Chieregato, A.; Hermans, I. Selective oxidative dehydrogenation of propane to propene using boron nitride catalysts. *Science* **2016**, *354*, 1570–1573. [CrossRef]
18. Boekfa, B.; Treesukol, P.; Injongkol, Y.; Maihom, T.; Maitarad, P.; Limtrakul, J. The Activation of Methane on Ru, Rh, and Pd Decorated Carbon Nanotube and Boron Nitride Nanotube: A DFT Study. *Catalysts* **2018**, *8*, 190. [CrossRef]
19. Dong, J.; Fu, Q.; Li, H.; Xiao, J.; Yang, B.; Zhang, B.; Bai, Y.; Song, T.; Zhang, R.; Gao, L.; et al. Reaction-Induced Strong Metal–Support Interactions between Metals and Inert Boron Nitride Nanosheets. *J. Am. Chem. Soc.* **2020**, *142*, 17167–17174. [CrossRef]

20. Yang, H.; Yu, R.; Fang, Y.; Yao, J.; Gan, Y.; Chen, J.; Deng, H.; Gao, X.; Zong, X.; Wang, J.; et al. Singly dispersed Ir1Ti3 bimetallic site for partial oxidation of methane at high temperature. *Appl. Surf. Sci.* **2022**, *599*, 153863. [CrossRef]

21. Wang, P.; Yao, J.; Jiang, Q.; Gao, X.; Lin, D.; Yang, H.; Wu, L.; Tang, Y.; Tan, L. Stabilizing the isolated Pt sites on PtGa/Al₂O₃ catalyst via silica coating layers for propane dehydrogenation at low temperature. *Appl. Catal. B Environ.* **2022**, *300*, 120731. [CrossRef]

22. Song, T.; Dong, J.; Li, R.; Xu, X.; Hiroaki, M.; Yang, B.; Zhang, R.; Bai, Y.; Xin, H.; Lin, L.; et al. Oxidative Strong Metal–Support Interactions between Metals and Inert Boron Nitride. *J. Phys. Chem. Lett.* **2021**, *12*, 4187–4194. [CrossRef] [PubMed]

23. Zhang, B.; Li, G.; Liu, S.; Qin, Y.; Song, L.; Wang, L.; Zhang, X.; Liu, G. Boosting propane dehydrogenation over PtZn encapsulated in an epitaxial high-crystallized zeolite with a low surface barrier. *ACS Catal.* **2022**, *12*, 1310–1314. [CrossRef]

24. Yang, K.; Liu, Q.; Zheng, Y.; Yin, H.; Zhang, S.; Tang, Y. Locally Ordered Graphitized Carbon Cathodes for High-Capacity Dual-Ion Batteries. *Angew. Chem. Int. Ed.* **2021**, *60*, 6326–6332. [CrossRef]

25. Paalanen, P.P.; van Vreeswijk, S.H.; Weckhuysen, B.M. Combined In Situ X-ray Powder Diffractometry/Raman Spectroscopy of Iron Carbide and Carbon Species Evolution in Fe(−Na–S)/α-Al₂O₃ Catalysts during Fischer–Tropsch Synthesis. *ACS Catal.* **2020**, *10*, 9837–9855. [CrossRef]

26. Roy, S.; Zhang, X.; Puthirath, A.B.; Meiyazhagan, A.; Bhattacharyya, S.; Rahman, M.M.; Babu, G.; Susarla, S.; Saju, S.K.; Tran, M.K.; et al. Structure, Properties and Applications of Two-Dimensional Hexagonal Boron Nitride. *Adv. Mater.* **2021**, *33*, 2101589. [CrossRef]

27. Han, R.; Diao, J.; Kumar, S.; Lyalin, A.; Taketsugu, T.; Casillas, G.; Richardson, C.; Liu, F.; Yoon, C.W.; Liu, H.; et al. Boron nitride for enhanced oxidative dehydrogenation of ethylbenzene. *J. Energy Chem.* **2021**, *57*, 477–484. [CrossRef]

28. Schild, D.; Ulrich, S.; Ye, J.; Stüber, M. XPS investigations of thick, oxygen-containing cubic boron nitride coatings. *Solid State Sci.* **2010**, *12*, 1903–1906. [CrossRef]

29. Gao, L.; Fu, Q.; Wei, M.; Zhu, Y.; Liu, Q.; Crumlin, E.; Liu, Z.; Bao, X. Enhanced Nickel-Catalyzed Methanation Confined under Hexagonal Boron Nitride Shells. *ACS Catal.* **2016**, *6*, 6814–6822. [CrossRef]

30. Kim, Y.; Kang, S.; Kang, D.; Lee, K.R.; Song, C.K.; Sung, J.; Kim, J.S.; Lee, H.; Park, J.; Yi, J. Single-Phase Formation of Rh₂O₃ Nanoparticles on h-BN Support for Highly Controlled Methane Partial Oxidation to Syngas. *Angew. Chem. Int. Ed.* **2021**, *60*, 25411–25418. [CrossRef]

31. Wang, Y.; Wang, J.; Zheng, P.; Sun, C.; Luo, J.; Xie, X. Boosting selectivity and stability on Pt/BN catalysts for propane dehydrogenation via calcination & reduction-mediated strong metal-support interaction. *J. Energy Chem.* **2022**, *67*, 451–457. [CrossRef]

32. Yan, G.; Tang, Y.; Li, Y.; Li, Y.; Nguyen, L.; Sakata, T.; Higashi, K.; Tao, F.F.; Sautet, P. Reaction product-driven restructuring and assisted stabilization of a highly dispersed Rh-on-ceria catalyst. *Nat. Catal.* **2022**, *5*, 119–127. [CrossRef]

33. Lang, R.; Li, T.B.; Matsumura, D.; Miao, S.; Ren, Y.J.; Cui, Y.T.; Tan, Y.; Qiao, B.T.; Li, L.; Wang, A.Q.; et al. Hydroformylation of Olefins by a Rhodium Single-Atom Catalyst with Activity Comparable to RhCl(PPh3)(3). *Angew. Chem.-Int. Ed.* **2016**, *55*, 16054–16058. [CrossRef] [PubMed]

34. Kwon, Y.; Kim, T.Y.; Kwon, G.; Yi, J.; Lee, H. Selective Activation of Methane on Single-Atom Catalyst of Rhodium Dispersed on Zirconia for Direct Conversion. *J. Am. Chem. Soc.* **2017**, *139*, 17694–17699. [CrossRef]

35. Matsubu, J.C.; Zhang, S.Y.; DeRita, L.; Marinkovic, N.S.; Chen, J.G.G.; Graham, G.W.; Pan, X.Q.; Christopher, P. Adsorbate-mediated strong metal-support interactions in oxide-supported Rh catalysts. *Nat. Chem.* **2017**, *9*, 120–127. [CrossRef]

36. Zhang, S.; Tang, Y.; Nguyen, L.; Zhao, Y.-F.; Wu, Z.; Goh, T.-W.; Liu, J.J.; Li, Y.; Zhu, T.; Huang, W.; et al. Catalysis on Singly Dispersed Rh Atoms Anchored on an Inert Support. *ACS Catal.* **2018**, *8*, 110–121. [CrossRef]

37. Jeong, H.; Lee, G.; Kim, B.-S.; Bae, J.; Han, J.W.; Lee, H. Fully Dispersed Rh Ensemble Catalyst to Enhance Low-Temperature Activity. *J. Am. Chem. Soc.* **2018**, *140*, 9558–9565. [CrossRef]

38. Guo, Q.; Wang, Y.; Han, J.; Zhang, J.; Wang, F. Interfacial Tandem Catalysis for Ethylene Carbonylation and C–C Coupling to 3-Pentanone on Rh/Ceria. *ACS Catal.* **2022**, *12*, 3286–3290. [CrossRef]

39. Bhattacharya, A.; Bhattacharya, S.; Das, G.P. Band gap engineering by functionalization of BN sheet. *Phys. Rev. B* **2012**, *85*, 035415. [CrossRef]

40. Sainsbury, T.; Satti, A.; May, P.; Wang, Z.; McGovern, I.; Gun'ko, Y.K.; Coleman, J. Oxygen Radical Functionalization of Boron Nitride Nanosheets. *J. Am. Chem. Soc.* **2012**, *134*, 18758–18771. [CrossRef]

41. Huang, R.; Zhang, B.; Wang, J.; Wu, K.-H.; Shi, W.; Zhang, Y.; Liu, Y.; Zheng, A.; Schlögl, R.; Su, D.S. Direct Insight into Ethane Oxidative Dehydrogenation over Boron Nitrides. *ChemCatChem* **2017**, *9*, 3293–3297. [CrossRef]

42. Kazansky, V.B.; Subbotina, I.R.; Pronin, A.A.; Schlögl, R.; Jentoft, F.C. Unusual Infrared Spectrum of Ethane Adsorbed by Gallium Oxide. *J. Phys. Chem. B* **2006**, *110*, 7975–7978. [CrossRef]

43. Wasylenko, W.; Frei, H. Direct Observation of Surface Ethyl to Ethane Interconversion upon C₂H₄ Hydrogenation over Pt/Al₂O₃ Catalyst by Time-Resolved FT-IR Spectroscopy. *J. Phys. Chem. B* **2005**, *109*, 16873–16878. [CrossRef] [PubMed]

44. Christian Enger, B.; Lødeng, R.; Holmen, A. A review of catalytic partial oxidation of methane to synthesis gas with emphasis on reaction mechanisms over transition metal catalysts. *Appl. Catal. A Gen.* **2008**, *346*, 1–27. [CrossRef]

45. Wang, D.; Dewaele, O.; Groote, A.M.D.; Froment, G.F. Reaction Mechanism and Role of the Support in the Partial Oxidation of Methane on Rh/Al$_2$O$_3$. *J. Catal.* **1996**, *159*, 418–426. [CrossRef]

46. Liu, X.; Zhang, S.; Zhao, H.; Lin, H.; Xu, K.; Xu, Y.; Tan, L.; Wu, L.; Tang, Y. In-situ studies on the synergistic effect of Pd-Mo bimetallic catalyst for anisole hydrodeoxygenation. *Mol. Catal.* **2022**, *530*, 112591. [CrossRef]